

M Times Photon Subtraction-Addition Coherent Superposition Operated Odd-Schrödinger-cat State: Nonclassicality and Decoherence

Li Huang, Qin Guo[†], Li-ying Jiang, Ge Chen, Xue-xiang Xu, Wen Yuan

¹College of Physics and Communication Electronics,

Jiangxi Normal University, Nanchang, 330022, China and

²Key Laboratory of Optoelectronic and Telecommunication of Jiangxi, Nanchang 330022, China

We introduce a new non-Gaussian state, generated by m times coherent superposition operation $a \cos \theta + a^\dagger e^{i\varphi} \sin \theta$ (MCSO) on odd-Schrödinger-cat state (OSCS). Its normalized constant is turned out to be related with the Hermite polynomial. We further investigate the nonclassical properties of the MCSO-OSCS through Mandel's Q-parameter, quadrature squeezing, the photocount distribution and Wigner function (WF). It is shown that the nonclassicality of the MCSO-OSCS is influenced by the number of times (m) of coherent superposition operation, the angle θ and the amplitude $|\alpha_0|$. Especially the volume of negative region of WF increases with the increment of parameters m , θ and α_0 . We also investigate the decoherence of the MCSO-OSCS in terms of the fadeaway of the negativity of WF in a thermal environment.

Keywords: Non-Gaussian state. Wigner function. Coherent Superposition Operation. odd-Schrödinger-cat state. Decoherence.

PACS: 0365, 0530, 4250

I. INTRODUCTION

Nonclassical states with non-Gaussian Wigner function (WF) have brought great interest in quantum optics and quantum information science [1]. For example, a single-photon state with non-Gaussian behavior in phase space has been found many applications in quantum information processing. In particular, any single-mode nonclassical state has become a sufficient resource to generate a two-mode entanglement via a beam-splitter [2]. Recently, the non-Gaussian states have attracted more attention of both experimentalists and theoreticians [3–7]. It is possible to generate and manipulate various non-Gaussian states through subtracting or adding photon operation or photon subtraction-addition coherent superposition operation on traditional quantum states or Gaussian states [8]. For example, the photon subtraction transforms a Gaussian entangled state (two-mode squeezed state) to a non-Gaussian entangled state for a nonlocality test [9] and entanglement distillation [10]. The photon addition can also transform a classical state to a nonclassical state [11]. In laboratory the operation of photon subtraction or addition is now realized practically [12, 13]. In Ref. [14], Lee *et al.* consider a coherent superposition of photon subtraction and addition, $ta + ra^\dagger$, acting on a coherent state and a thermal state to form non-Gaussian states, and propose the experimental scheme to implement this elementary coherent operation. Furthermore, other non-Gaussian state is obtained theoretically through m times coherent superposition of photon subtraction and addition, $(ta + ra^\dagger)^m$, acting on thermal state [15] and coherent state [16], respectively.

On the other hand, as a kind of nonclassical state, the so-called Schrödinger cat states (SCS, quantum superpositions of coherent states [17]), play an important role in fundamental tests of quantum theory [18, 19] and in many quantum information processing tasks, including quantum computation [20], quantum teleportation [21] and precision measurements [22, 23]. There have been a great deal of theoretical and experimental attempts to generate a Schrödinger-cat-type state and considerable experimental progresses have been achieved in recent years [24–28]. Such as in Ref. [28] a Schrödinger-cat-like state is generated via a coherent superposition of photonic operations.

Thus an interesting question is naturally raised: can we operate the coherent superposition operator $(a \cos \theta + a^\dagger e^{i\varphi} \sin \theta)^m$ on odd-Schrödinger-cat state (OSCS) to construct a new non-Gaussian quantum state? The answer is definite. Considering the above reasons, we shall construct a new nonclassical state (MCSO-OSCS) which is supposed to be realized in experiment. In this paper, We focus on studying its nonclassical properties of this state by deriving analytically some expressions, such as normalized constant, sub-Poissonian statistics, photocount distribution and Wigner function. In fact, systems are usually surrounded by a thermal reservoir, and decoherence becomes an important topic in the fields of quantum optics. Enlightened by these ideas, we shall also discuss its decoherence property in a thermal environment in this paper.

The paper is organized as follows. In Sec. 2, the MCSO-OSCS is constructed and its normalized constant turns out to be related with the Hermite polynomial. In Sec. 3, the fidelity between MCSO-OSCS and its original state (OSCS) shall be obtain. In Sec. 4, the nonclassical properties of the MCSO-OSCS, such as sub-Poissonian statistics, quadrature squeezing properties and photocount distribution are calculated analytically and then discussed in details. In Sec.5, the explicitly analytical expression of WF for the MCSO-OSCS is derived. According to the negativity of WF, the nonclassical properties are also discussed in details. In Sec. 6, the decoherence of the MCSO-OSCS in a thermal

environment is investigated. In Sec. 7, we end our work with main conclusions.

II. NORMALIZATION OF THE MCSO-OSCS

Theoretically, the MCSO-OSCS can be introduced by repeated application of coherent superposition operator Ω to the OSCS ($|\alpha_0\rangle - |-\alpha_0\rangle$) for m times, i.e.,

$$|\psi_m\rangle = \Omega^m (|\alpha_0\rangle - |-\alpha_0\rangle), \quad (1)$$

where $\Omega = a \cos \theta + a^\dagger e^{i\varphi} \sin \theta$ with $[a, a^\dagger] = 1$ and $\theta \in (0, \pi/2)$, m is the order of coherent superposition operator (a non-negative integer), $|\alpha_0\rangle$ is a coherent state of amplitude $|\alpha_0|$. The density operator of the MCSO-OSCS is $\rho_m = N_m^{-1} |\psi_m\rangle \langle \psi_m|$, where N_m is a normalized constant of the MCSO-OSCS to be determined by $\text{Tr} \rho_m = 1$. If Ω^m operates on the even SCS ($|\alpha_0\rangle + |-\alpha_0\rangle$), then we obtain the MCSO-ESCS. We only discuss the properties of MCSO-OSCS in this paper, for an odd SCS in general show stronger nonclassical properties than an even SCS [29].

In order to obtain the normalized constant N_m , and note that the operator Ω is not always Hermitian due to $\Omega \neq \Omega^\dagger$ when $\cos \theta \neq e^{i\varphi} \sin \theta$, we shall derive the normal ordering form of Ω^m firstly. Recalling the generating function of the Hermite polynomial $H_m(x)$ [30], i.e. $\sum_{m=0}^{\infty} \frac{t^m}{m!} H_m(x) = \exp(2xt - t^2)$, with

$$H_m(x) = \sum_{l=0}^{[m/2]} \frac{(-1)^l m! (2x)^{m-2l}}{l! (m-2l)!} = \frac{\partial^m}{\partial t^m} \exp(2xt - t^2) \Big|_{t=0}, \quad (2)$$

using the Baker-Hausdorff formula $e^{A+B} = e^A e^B e^{-\frac{1}{2}[A,B]} = e^B e^A e^{-\frac{1}{2}[B,A]}$ [31] and the technique of integration within an ordered product (IWOP) of operators [32], we have

$$\begin{aligned} e^{\lambda \Omega} &= : e^{\lambda \Omega + \frac{1}{2} \lambda^2 e^{i\varphi} \sin \theta \cos \theta} : \\ &= \sum_{m=0}^{\infty} \frac{\lambda^m \left(-i \sqrt{\frac{1}{2} e^{i\varphi} \sin \theta \cos \theta} \right)^m}{m!} : H_m \left(\frac{i\Omega}{\sqrt{2e^{i\varphi} \sin \theta \cos \theta}} \right) : , \end{aligned} \quad (3)$$

where the symbol $: :$ stands for the normally ordering. Comparing Eq.(3) with the expansion of $e^{\lambda \Omega}$, i.e. $e^{\lambda \Omega} = \sum_{m=0}^{\infty} \frac{\lambda^m}{m!} \Omega^m$, we can easily obtain the normal ordering form of Ω^m :

$$\Omega^m = \left(-i \sqrt{\frac{1}{2} e^{i\varphi} \sin \theta \cos \theta} \right)^m : H_m \left(\frac{i\Omega}{\sqrt{2e^{i\varphi} \sin \theta \cos \theta}} \right) : . \quad (4)$$

Similarly, $\Omega^{\dagger m} = (a^\dagger \cos \theta + a e^{-i\varphi} \sin \theta)^m$ has the normal ordering form as follows:

$$\Omega^{\dagger m} = \left(-i \sqrt{\frac{1}{2} e^{-i\varphi} \sin \theta \cos \theta} \right)^m : H_m \left(\frac{i\Omega^\dagger}{\sqrt{2e^{-i\varphi} \sin \theta \cos \theta}} \right) : . \quad (5)$$

From Eq. (4) and (5), we also give the following relations

$$\langle \beta | \Omega^m | \alpha \rangle = \left(-i \sqrt{\frac{1}{2} e^{i\varphi} \sin \theta \cos \theta} \right)^m H_m \left(\frac{i(\alpha \cos \theta + \beta^* e^{i\varphi} \sin \theta)}{\sqrt{2e^{i\varphi} \sin \theta \cos \theta}} \right) \langle \beta | \alpha \rangle , \quad (6)$$

and

$$\langle \beta | \Omega^{\dagger m} | \alpha \rangle = \left(-i \sqrt{\frac{1}{2} e^{-i\varphi} \sin \theta \cos \theta} \right)^m H_m \left(\frac{i(\beta^* \cos \theta + \alpha e^{-i\varphi} \sin \theta)}{\sqrt{2e^{-i\varphi} \sin \theta \cos \theta}} \right) \langle \beta | \alpha \rangle , \quad (7)$$

where $|\alpha\rangle$ and $|\beta\rangle$ are coherent states and $\langle \beta | \alpha \rangle = \exp \left[-\frac{1}{2} (|\alpha|^2 + |\beta|^2) + \beta^* \alpha \right]$ [33, 34]. Eq. (6) and (7) are very useful in the following calculations.

Next, according to $\text{Tr}\rho_m = 1$, we obtain

$$N_m = \text{Tr} [|\psi_m\rangle \langle \psi_m|] = \langle \psi_m | \psi_m \rangle. \quad (8)$$

Substituting Eq. (1), (4)-(5) into (8), and inserting the completeness relation of the coherent state $\int \frac{d^2z}{\pi} |z\rangle \langle z| = 1$, furthermore, with the help of Eq. (2) and the following integral formula

$$\begin{aligned} & \int \frac{d^2z}{\pi} \exp \left(\zeta |z|^2 + \xi z + \eta z^* + f z^2 + g z^{*2} \right) \\ &= \frac{1}{\sqrt{\zeta^2 - 4fg}} \exp \left(\frac{-\zeta\xi\eta + \xi^2g + \eta^2f}{\zeta^2 - 4fg} \right), \end{aligned} \quad (9)$$

whose convergent condition is $\text{Re}(\zeta \pm f \pm g) < 0$, $\text{Re}[(\zeta^2 - 4fg)/(\zeta \pm f \pm g)] < 0$, we obtain

$$N_m = 2\chi^m \left[\sum_{k=0}^m (-1)^m A |H_{m-k}(B)|^2 - \sum_{k=0}^m (-1)^k A |H_{m-k}(C)|^2 \exp(-2|\alpha_0|^2) \right], \quad (10)$$

where we have set

$$\begin{aligned} A &= \left(2 \frac{\sin \theta}{\cos \theta} \right)^k \frac{1}{k!} \left(\frac{m!}{(m-k)!} \right)^2, \\ B &= i \sqrt{\frac{e^{-i\varphi} \sin \theta}{2 \cos \theta}} \alpha_0 + \frac{i \sqrt{e^{i\varphi} \cos \theta}}{\sqrt{2 \sin \theta}} \alpha_0^*, \\ C &= \frac{i \sqrt{e^{-i\varphi} \cos \theta}}{\sqrt{2 \sin \theta}} \alpha_0 - \frac{i \sqrt{e^{i\varphi} \sin \theta}}{\sqrt{2 \cos \theta}} \alpha_0^*, \\ \chi &= -\frac{1}{2} \sin \theta \cos \theta, \end{aligned} \quad (11)$$

and we have used the recurrence relation of $H_m(x)$:

$$\frac{\partial}{\partial x^l} H_m(x) = \frac{2^l m!}{(m-l)!} H_{m-l}(x). \quad (12)$$

Eq.(10) indicates that the normalization factor N_m is just related to a Hermite polynomial. Obviously, when $m = 0$, the MCSO-OSCS just reduces to the odd SCS. The analytical expression of N_m is important for further investigating the properties of MCSO-OSCS. For MCSO-ESCS, we can change the negative sign "−" before the second sign of sum in Eq.(10) to the positive sign "+" and obtain its normalized constant.

III. FIDELITY BETWEEN MCSO-OSCS AND OSCS

In quantum teleportation, the fidelity F , which measures how close the teleported state is to the original state, is the projection of the original pure state $|\Psi_{in}\rangle$ of the density operator $\rho_{in} = |\Psi_{in}\rangle \langle \Psi_{in}|$ onto the teleported state $|\Psi_{out}\rangle$ of the density operator ρ_{out} : $F = \text{Tr}(\rho_{out}\rho_{in})$ [35, 36]. Here the fidelity measures how close the new state (MCSO-OSCS) is to the original state (OSCS). The fidelity between MCSO-OSCS (density matrix is ρ_m) and its original OSCS (ρ_o) is defined as [8]

$$F_{\theta, \varphi, m} = \frac{\text{Tr}(\rho_m \rho_o)}{\text{Tr}(\rho_o^2)}. \quad (13)$$

In general, $0 \leq F \leq 1$, and $F = 1$ shows that the two states are same, while $F = 0$ shows that the two states are anamorphic absolutely. Employing the similar procedure of deriving the normalization constant, the fidelity for MCSO-OSCS can be calculated out as

$$F_{\theta, \varphi, m} = \frac{N_m^{-1} \chi^m}{4(1 - e^{-2|\alpha_0|^2})^2} \left| [(-1)^m + 1] \left[H_m(B^*) - e^{-2|\alpha_0|^2} H_m(C) \right] \right|^2. \quad (14)$$

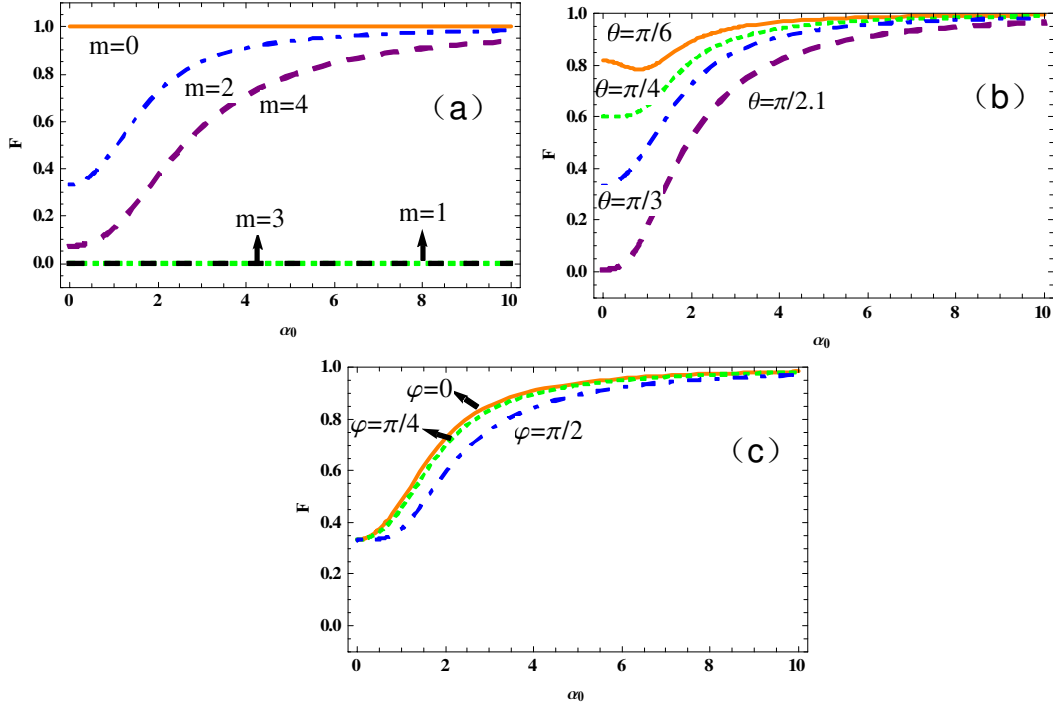


FIG. 1: Fidelity between MCSO-OSCS and OSCS as a function of α_0 (here α_0 is setted as real number) (a) $\theta = \frac{\pi}{3}$, $\varphi = 0$, with different m values; (b) $m = 2$, $\varphi = 0$, with different θ values; (c) $m = 2$, $\theta = \frac{\pi}{3}$, with different φ values.

In particular, when $m = 0$, leading to $\rho_m = \rho_o$, then Eq. (13) reduces to $F_{\theta,\varphi,m} = 1$ (see Fig.1(a)), which indicates that the MCSO-OSCS is reduced to the OSCS, as expected. In Eq. (14) the fidelity $F_{\theta,\varphi,m}$ is equal to 0 as m is an odd number because of the term $((-1)^m + 1)$. In Fig.1(a), we plot the fidelity $F_{\theta,\varphi,m}$ as the function of α_0 for some different m values with some given θ, φ values, here α_0 is setted as a real number, the same as in Figs. 2, 3, 8. It is obvious to note that $F_{\theta,\varphi,m} = 0$ when $m = 1, 3$, as expected, and $F_{\theta,\varphi,m} \neq 0$ when $m = 2, 4$. When m is an even number, the fidelity increases monotonously with the increment of α_0 and tends to 1 finally, which indicates that the coherent superposition operation has no influence on the field when the field is strong enough. Comparing with the curves of $m = 0, 2, 4$, we find that the smaller the value of m is, the bigger the fidelity is. In order to see the effect of different θ values on the fidelity, we plot the fidelity as the function of α_0 for some different θ values and given m, φ values, see Fig.1(b). It is shown that the fidelity decreases as θ increases. In addition, we study the relation of the fidelity and parameter φ through the plot of Fig.1(c). It is shown that the values of parameter φ have little influence on the fidelity. It is also shown that the fidelity increases as the amplitude α_0 increases from Fig.1(b) and 1(c).

IV. NONCLASSICAL PROPERTIES OF MCSO-OSCS

In this section, we shall discuss the nonclassical properties of the MCSO-OSCS in terms of sub-Poissonian statistics, quadrature squeezing properties and the negativity of its Wigner function.

A. Mandel's Q-parameter

The Mandel's Q-parameter measures the deviation of the variance of the photon number distribution of the field state under consideration from the Poissonian distribution of the coherent state, which has been defined as [37]

$$Q = \frac{\langle a^{\dagger 2} a^2 \rangle}{\langle a^{\dagger} a \rangle} - \langle a^{\dagger} a \rangle. \quad (15)$$

The quantum states has the Poissonian, sub-Poissonian and super-Poissonian statistics for $Q = 0, Q < 0$ and $Q > 0$, respectively. It is well known that the negativity of Q-parameter refers to the nonclassical character of the state, but a

state may be nonclassical even though Q -parameter is positive as pointed out in [38].

Using Eqs.(4), (5), $\rho_m = N_m^{-1} |\psi_m\rangle \langle \psi_m|$ and IWOP technique of operators, one can calculate $\langle a^\dagger a \rangle$ as

$$\begin{aligned} \langle a^\dagger a \rangle &= \text{Tr}(\rho_m a^\dagger a) \\ &= N_m^{-1} \chi^m \sum_{k=0}^m I \left[\begin{aligned} &+ (-1)^{m-k} (k+1 + |\alpha_0|^2) |H_{m-k}(B)|^2 \\ &- (k+1 - |\alpha_0|^2) |H_{m-k}(C)|^2 e^{-2|\alpha_0|^2} \\ &+ 2 \text{Re}[R^* \alpha_0^* (m-k) H_{m-k}(-B) H_{m-k-1}(B^*)] \\ &- 2 \text{Re}[R^* \alpha_0^* (m-k) H_{m-k}(C^*) H_{m-k-1}(C) e^{-2|\alpha_0|^2}] \end{aligned} \right] - 1, \end{aligned} \quad (16)$$

where

$$\begin{aligned} R &= \frac{i\sqrt{2e^{-i\varphi} \sin \theta}}{\sqrt{\cos \theta}}, \\ I &= \frac{2}{k!} \left(\frac{m!}{(m-k)!} \right)^2 (-|R|^2)^k, \end{aligned} \quad (17)$$

and get the value of $\langle a^2 a^{\dagger 2} \rangle$ as

$$\langle a^2 a^{\dagger 2} \rangle = f_1(\alpha_0) + f_1(-\alpha_0) - f_2(\alpha_0) - f_2(-\alpha_0), \quad (18)$$

where

$$\begin{aligned} f_1(\alpha_0) &= N_m^{-1} \chi^m \frac{\partial^{2m+2}}{\partial t^m \partial s^m \partial \lambda \partial \eta} \frac{e^{-|\alpha_0|^2 - K^* t + K s - s^2 - t^2}}{\sqrt{1-4\lambda\eta}} e^{(H+H_0+|\alpha_0|^2)/(1-4\lambda\eta)} \Big|_{s=t=\lambda=\eta=0}, \\ f_2(\alpha_0) &= N_m^{-1} \chi^m \frac{\partial^{2m+2}}{\partial t^m \partial s^m \partial \lambda \partial \eta} \frac{e^{-|\alpha_0|^2 - K^* t - K s - s^2 - t^2}}{\sqrt{1-4\lambda\eta}} e^{(H-L_0-|\alpha_0|^2)/(1-4\lambda\eta)} \Big|_{s=t=\lambda=\eta=0}, \end{aligned} \quad (19)$$

and

$$\begin{aligned} K &= i \frac{\sqrt{2e^{-i\varphi} \cos \theta}}{\sqrt{\sin \theta}} \alpha_0, \\ H &= -|R|^2 t s + R^2 t^2 \eta + \alpha_0^{*2} \eta + \alpha_0^2 \lambda + R^{*2} s^2 \lambda, \\ H_0 &= R \alpha_0 t - R^* \alpha_0^* s + 2R \alpha_0^* t \eta - 2R^* \alpha_0 \lambda s, \\ L_0 &= R \alpha_0 t + R^* \alpha_0^* s - 2R \alpha_0^* t \eta - 2R^* \alpha_0 \lambda s. \end{aligned} \quad (20)$$

Here s, t, λ, η are parameters introduced into the calculation process and will be eliminated after finishing the calculation by setting them to zero. Furthermore, one can use the relation $[a, a^\dagger] = 1$ to obtain

$$\langle a^{\dagger 2} a^2 \rangle = \langle a^2 a^{\dagger 2} \rangle - 4 \langle a^\dagger a \rangle - 2. \quad (21)$$

Substituting Eqs. (16), and (21) into (15), and using the method of numerical calculation we can study the property of Mandel's Q -parameter for the MCSO-OSCS. The Q -parameters of MCSO-OSCS as the function of α_0 are depicted in Fig. 2 for several different values of m, θ and φ . It is interesting to note that the values of Q -parameter are always smaller than zero for different m values under the given $\theta = \frac{\pi}{4}$ and $\varphi = 0$ (see Fig. 2(a)), which indicates sub-Poissonian statistics. In addition, the absolute value of Q -parameter decreases with the increment of α_0 till tends to zero, which indicates that all states under different m values will tend to the Poissonian statistics (the distribution of a coherent state) when the value of α_0 is big enough. However, we can see that the range of the Q -parameter is $[-1, 0.5]$ in Fig. 2(b) with different m values and for given $\theta = \frac{\pi}{8}$ and $\varphi = 0$. That indicates the MCSO-OSCS with small value of θ may do not exhibit sub-Poissonian statistics but exhibit super-Poissonian statistics.

In particular, when $m = 1$ and $\varphi = 0$, the MCSO-OSCS deduces to the COSCS ($\Omega(|\alpha_0\rangle - |-\alpha_0\rangle)$) [29]. From Fig. 2(c), We can see that the range of the Q -parameter is $[-1, 0.7]$. From the criteria of Q -parameter, one finds that the MCSO-OSCS exhibits the sub-Poissonian statistics for $\theta = \frac{\pi}{4}, \frac{\pi}{3}$ and $\frac{\pi}{2.1}$. In the area of $\theta \in (0, \frac{\pi}{2})$, the bigger the value of θ is, the more chance the state exhibits the sub-Poissonian statistics. The similar conclusion can also be seen in Ref. [29]. In addition, from Fig. 2(d) we can see that the absolute value of Q -parameter decreases as φ increases, but this difference is not obvious.

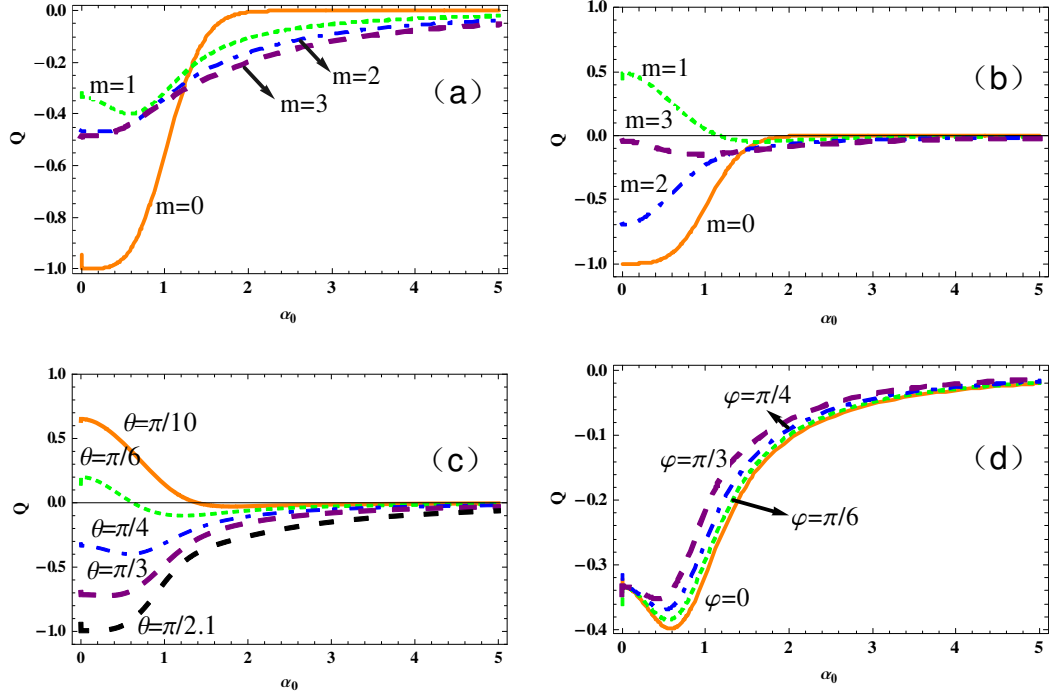


FIG. 2: Mandel's Q-parameter of MCSO-OSCS as a function of α_0 (a) $\theta = \frac{\pi}{4}$, $\varphi = 0$, with different m values; (b) $\theta = \frac{\pi}{8}$, $\varphi = 0$, with different m values; (c) $m = 1$, $\varphi = 0$, with different θ values; (d) $m = 1$, $\theta = \frac{\pi}{4}$, with $\varphi = \frac{\pi}{3}, \frac{\pi}{4}, \frac{\pi}{6}, 0$ (from upper to lower curves).

B. Quadrature squeezing properties of MCSO-OSCS

One observes nonclassical effects not only through sub-Poissonian statistics but also through squeezing effects, which do not allow classical interpretation of photoelectric counting events. Here, we consider an appropriate quadrature operator $X_\theta = ae^{-i\theta} + a^\dagger e^{i\theta}$, and the squeezing can be characterized by $\langle (\Delta X_\theta)^2 \rangle_{\min} < 1$ with respect to angle θ , or by the normal ordering form $\langle : (\Delta X_\theta)^2 : \rangle_{\min} < 0$ [39]. Upon expanding the terms in $\langle : (\Delta X_\theta)^2 : \rangle_{\min}$, one can minimize its value over the whole angle θ , which is given by [40]

$$S = \langle : (\Delta X_\theta)^2 : \rangle_{\min} = -2 \left| \langle a^{\dagger 2} \rangle - \langle a^\dagger \rangle^2 \right| + 2 \langle a^\dagger a \rangle - 2 |\langle a^\dagger \rangle|^2. \quad (22)$$

Then its negative value in the range $[-1, 0)$ indicates squeezing (or nonclassicality). Similarly, using the integration formula (9), we obtain

$$\langle a^\dagger \rangle = 0, \quad (23)$$

and

$$\langle a^{\dagger 2} \rangle = f_3(\alpha_0) + f_3(-\alpha_0) - f_4(\alpha_0) - f_4(-\alpha_0), \quad (24)$$

where

$$\begin{aligned} f_3(\alpha_0) &= N_m^{-1} \chi^m \frac{\partial^{2m}}{\partial t^m \partial s^m} (Rt + \alpha_0^*)^2 e^{-t^2 - s^2 - |R|^2 st + 2Bt - 2B^* s} \Big|_{s=t=0}, \\ f_4(\alpha_0) &= N_m^{-1} \chi^m \frac{\partial^{2m}}{\partial t^m \partial s^m} (Rt + \alpha_0^*)^2 e^{-t^2 - s^2 - |R|^2 st - 2C^* t - 2Cs - 2| \alpha_0|^2} \Big|_{s=t=0}. \end{aligned} \quad (25)$$

Using Eqs.(16), (23), (24) and (22), one can obtain the expression of the quadrature squeezing S of MCSO-OSCS.

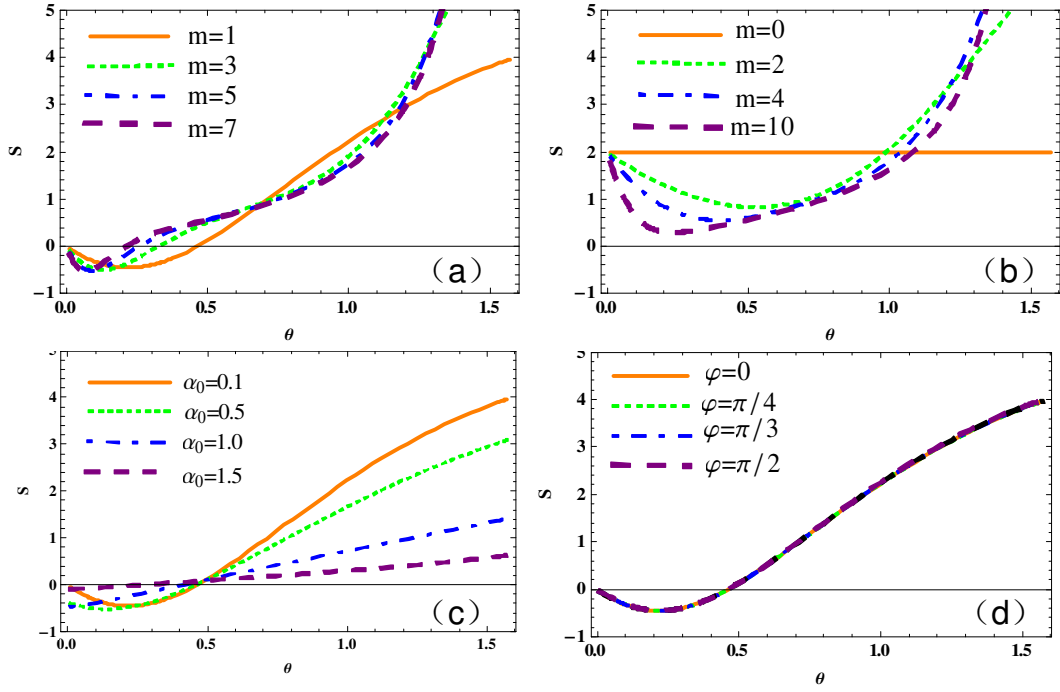


FIG. 3: Quadrature squeezing of MCSO-OSCS as a function of θ (a) $\alpha_0 = 0.1$, $\varphi = 0$, with different m values; (b) $\alpha_0 = 0.1$, $\varphi = 0$, with different m values; (c) $m = 1$, $\varphi = 0$, with different α_0 values; (d) $m = 1$, $\alpha_0 = 0.1$, with different φ values.

We plot the graph of quadrature squeezing S as a function of θ for some different m values and for given φ and α_0 values, (say $\varphi = 0$ and $\alpha_0 = 0.1$), see Fig. 3(a) and (b). It is interesting to find that the MCSO-OSCS can exhibit squeezing when the parameter m is odd ($m = 1, 3, 5, 7$) and the angle θ is smaller than a threshold, while can't exhibit squeezing when the parameter m is even ($m = 0, 2, 4, 10$) for any angle θ . Furthermore, we find that the original state ($m = 0$) can't exhibit squeezing, which implies that the odd times coherent superposition operation (Ω^m , m is odd.) can achieve squeezing. Small angle θ corresponds to the case that the subtracting photon operation is in the ascendant, which indicates that subtracting photon operation is benefit to squeezing under the case of odd m .

In Fig. 3(c), we plot the graph of S as a function of θ for some different α_0 values and for given φ and m values, (say $\varphi = 0$ and $m = 1$). We find that small value of α_0 is helpful to squeezing on condition that the angle θ is smaller than a threshold. From Fig. 3(d), We can see that different φ values have no effect on the squeezing of MCSO-OSCS.

C. Photocount Distribution of MCSO-OSCS

For the case of a single radiation mode of registering n photoelectrons in the time interval T , the photon counting distribution $P(n)$ is given by [41],

$$P(n) = \text{Tr} \left[\rho: \frac{(\xi a^\dagger a)^n}{n!} e^{-\xi a^\dagger a} : \right], \quad (26)$$

where $\xi \propto T$ is called the quantum efficiency (a measure) of the detector, ρ is a single-mode density operator of the light field concerned. When $\xi = 1$, $P(n)$ becomes the photon number distribution (PND) for a given state. By virtue of the technique of IWOP of operators, Fan and Hu deduce a reformed formula as showed in reference [42],

$$P(n) = \frac{\xi^n}{(\xi - 1)^n} \int \frac{d^2 z}{\pi} e^{-\xi |z|^2} L_n(|z|^2) Q(\sqrt{1 - \xi} z), \quad (27)$$

where $Q(\beta) = \langle \beta | \rho | \beta \rangle$ is the Q-function, $|\beta\rangle$ is the coherent state, and $L_n(x)$ is the Laguerre polynomials. Once the Q-function of ρ is known, it is easy to calculate the photocount distribution of MCSO-OSCS from Eq.(27).

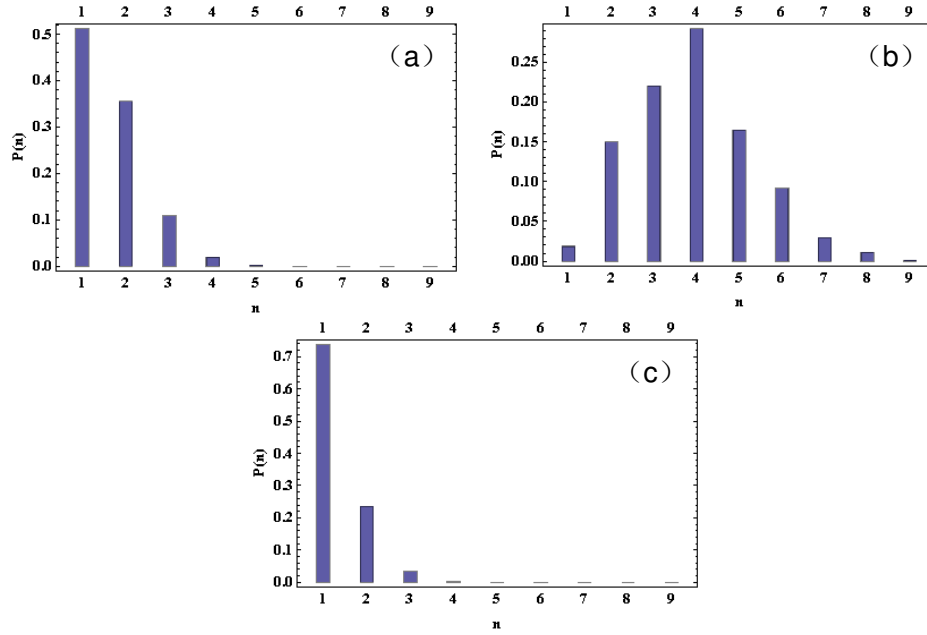


FIG. 4: Photocount distribution of MCSO-OSCS as a function of n (a non-negative integer) for $\alpha_0 = 0.5 + i0.5$ (a) $m = 4, \theta = \frac{\pi}{4}, \varphi = 0, \xi = 0.2$; (b) $m = 4, \theta = \frac{\pi}{4}, \varphi = 0, \xi = 0.9$; (c) $m = 1, \theta = \frac{\pi}{4}, \varphi = 0, \xi = 0.2$.

The Q-function of MCSO-OSCS is given by

$$\begin{aligned} Q(\beta) &= \langle \beta | \rho_m | \beta \rangle \\ &= N_m^{-1} \chi^m (\langle \beta | : H_m(a, a^\dagger) : (|\alpha_0\rangle - |-\alpha_0\rangle) (\langle \alpha_0| - \langle -\alpha_0|) : H_m^*(a, a^\dagger) : | \beta \rangle), \end{aligned} \quad (28)$$

where $H_m(a, a^\dagger) = H_m(i\Omega/\sqrt{2}e^{i\varphi} \sin \theta \cos \theta)$. Then substituting Eq.(28) into Eq.(27) and using Eq.(9) and the two-variable Hermite polynomials expression of Laguerre polynomials [30]

$$L_n(zz^*) = \frac{(-1)^n}{n!} H_{n,n}(z, z^*) = \frac{(-1)^n}{n!} \left. \frac{\partial^{2n}}{\partial \mu^n \partial \nu^n} e^{-\mu\nu + \mu z + \nu z^*} \right|_{\mu=\nu=0}, \quad (29)$$

we obtain the final result of $P(n)$

$$P(n) = 2T_{m,n} \sum_{j=0}^m \sum_{l,k=0}^n A_{j,k} \left[\begin{array}{c} e^{-\xi|\alpha_0|^2} H_{m-l-j}\left(\frac{K-J^*}{2}\right) H_{m-j-k}\left(\frac{J-K^*}{2}\right) \\ - (-1)^{n-k} e^{(\xi-2)|\alpha_0|^2} H_{m-l-j}\left(\frac{K^*+J}{2}\right) H_{m-j-k}\left(\frac{K+J^*}{2}\right) \end{array} \right], \quad (30)$$

where we have set

$$\begin{aligned} A_{j,k} &= \frac{(-1)^{j+k} G^{j+l} G^{*j+k} F^{n-l} F^{*n-k}}{l!j!k!(m-l-j)!(n-l)!(n-k)!(m-j-k)!}, \\ F &= \sqrt{1-\xi}\alpha_0, G = -\sqrt{1-\xi}R^*, \\ J &= (1-\xi)R\alpha_0, T_{m,n} = N_m^{-1} \chi^m \frac{n!(m!)^2 \xi^n}{(1-\xi)^n}. \end{aligned} \quad (31)$$

In order to discuss the photocount distribution of MCSO-OSCS, we plot the graph of $P(n)$ for several given parameters $\varphi, \theta, \alpha_0, m$, or ξ in Figs. 4 and 5. Comparing with Figs. 4(a) and (b), we find that for some given values of m, α_0, φ , and θ , the corresponding probability-peak of photocount distribution moves from $n=1$ to $n=4$ as $\xi=0.2$ increases to 0.9, which means that the probability of registering big photon-numbers is increasing gradually while the probability of registering small photon-numbers is decreasing when we increase the time interval T . Meanwhile, the larger the ξ is, the wider tail of photocount distribution of MCSO-OSCS has. We can also see that the probability of finding big photon-numbers increases with the increment of the parameter m (see Figs. 4(a) and 4(c)) or θ (see Figs. 4(b) and 5(a)). Similarly, the probability of finding big photon-numbers increases with the increment of parameter φ (see Figs. 5(a) and 5(b)).

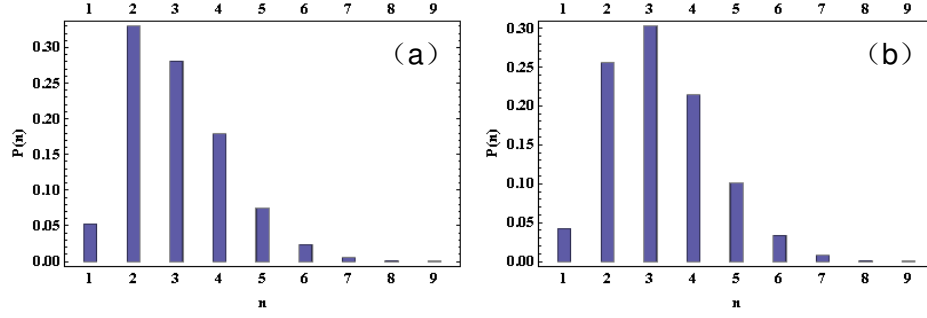


FIG. 5: Photocount distribution of MCSO-OSCS as a function of n (a non-negative integer) for $\alpha_0 = 0.5 + i0.5$ (a) $m = 4, \theta = \frac{\pi}{8}, \varphi = 0, \xi = 0.9$; (b) $m = 4, \theta = \frac{\pi}{8}, \varphi = \frac{\pi}{2}, \xi = 0.9$.

V. WIGNER FUNCTION OF THE MCSO-OSCS

The WF is a quasi-probability distribution, which fully describes the state of a quantum system in phase space. The partial negativity of the WF is indeed a good indication of the highly nonclassical character of the state [43]. Therefore it is worth obtaining the WF for any states and using the negative region to check whether a state has nonclassicality. For a single-mode system, the WF $W(\alpha, \alpha^*)$ associated with a quantum state density matrix ρ can be expressed as [44]:

$$W(\alpha) = \frac{1}{\pi} e^{2|\alpha|^2} \int \frac{d^2 z}{\pi} \langle -z | \rho | z \rangle e^{-2(\alpha^* z - \alpha z^*)}, \quad (32)$$

where $|z\rangle$ is the coherent state. Substituting $\rho_m = N_m^{-1} |\psi_m\rangle \langle \psi_m|$ into Eq.(32), we can finally obtain the WF of MCSO-OSCS:

$$W(\alpha) = W_{\alpha_0}(\alpha) + W_{-\alpha_0}(\alpha) - W'_{\alpha_0}(\alpha) - W'_{-\alpha_0}(\alpha), \quad (33)$$

where we have set

$$\begin{aligned} W_{\alpha_0}(\alpha) &= \sum_{k=0}^m D_m (-1)^k e^{-2|\alpha - \alpha_0|^2} |H_{m-k}(-C^* + R\alpha)|^2, \\ W'_{\alpha_0}(\alpha) &= \sum_{k=0}^m D_m (-1)^m e^{2\alpha_0^* \alpha - 2\alpha^* \alpha_0 - 2|\alpha|^2} H_{m-k}(B^* - R^* \alpha^*) H_{m-k}(B + R\alpha), \end{aligned} \quad (34)$$

and

$$D_m = \frac{1}{\pi} N_m^{-1} \left(\frac{1}{2} \sin \theta \cos \theta \right)^m \left(2 \frac{\sin \theta}{\cos \theta} \right)^k \frac{1}{k!} \left(\frac{m!}{(m-k)!} \right)^2. \quad (35)$$

It is found that the sum of $W'_{\alpha_0}(\alpha)$ and $W'_{-\alpha_0}(\alpha)$ is a real function due to $W'_{-\alpha_0}(\alpha) = [W'_{\alpha_0}(\alpha)]^*$. By using Eq. (33), the WFs as a function of real and imaginary parts of α for several different values of m, α_0 and θ are depicted in Figs. 6 and 7.

We can see clearly that the figures of WF distribution are non-Gaussian. In addition, as evidence of the nonclassicality of the state, it is easy to see that there is a negative region of the WF in each plot. From Fig. 6, We can see that the figures of WF exist odd (even) negative peaks when the values of m are even (odd) for given α_0, φ and θ , and exhibit more vibration character as the value of m increasing. Meanwhile, we can find that the minimum value of the WF occurs at the center of the figure when m is an even number (see Fig. 6(a) and Fig. 6(c)). But the case is not true when m is an odd number (see Fig. 6(b) and Fig. 6(d)). Comparing Fig. 6(c) ($\theta = \frac{\pi}{3}, m = 2, \alpha_0 = 1 + i$) with Fig. 7(a) ($\theta = \frac{\pi}{8}, m = 2, \alpha_0 = 1 + i$), we can see that the width of the figure of WF in one direction increases as increasing the value of θ . Comparing Fig. 6(c) ($\alpha_0 = 1 + i, m = 2, \theta = \frac{\pi}{3}$) with Fig. 7(b) ($\alpha_0 = 2 + 2i, m = 2, \theta = \frac{\pi}{3}$), we can also see that the figure of WF also exhibits more vibration character as increasing the value of amplitude $|\alpha_0|$.

The volume of the negative part of the WF were used in [45, 46] to describe the interference effects which determine the departure from classical behavior. In order to further evaluate how these parameters m, α_0 , and θ affect the

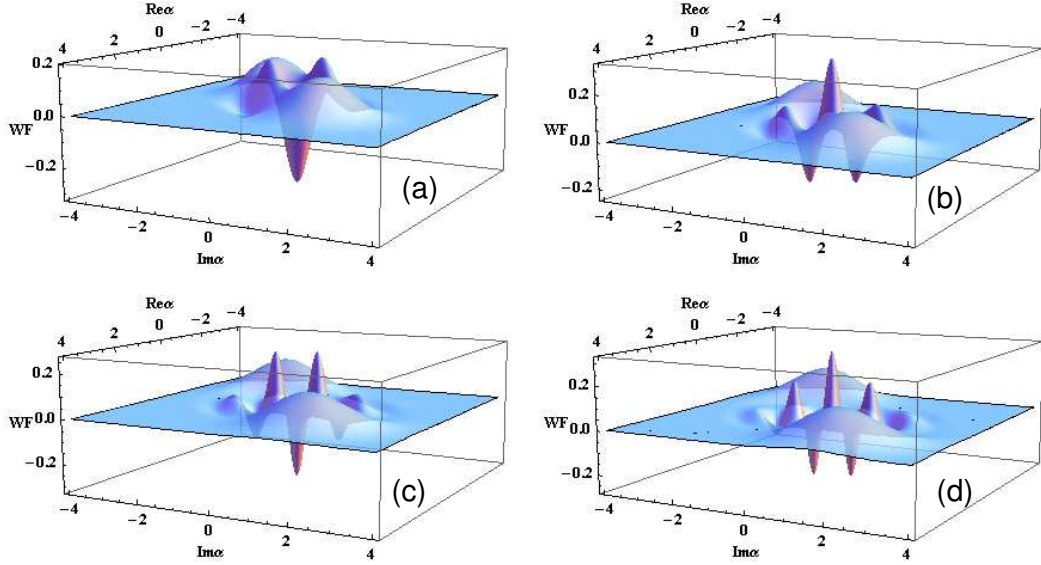


FIG. 6: Wigner function distributions of MCSO-OSCS with $\varphi = 0, \theta = \frac{\pi}{3}, \alpha_0 = 1 + i$ (a) $m = 0$; (b) $m = 1$; (c) $m = 2$; (d) $m = 3$.

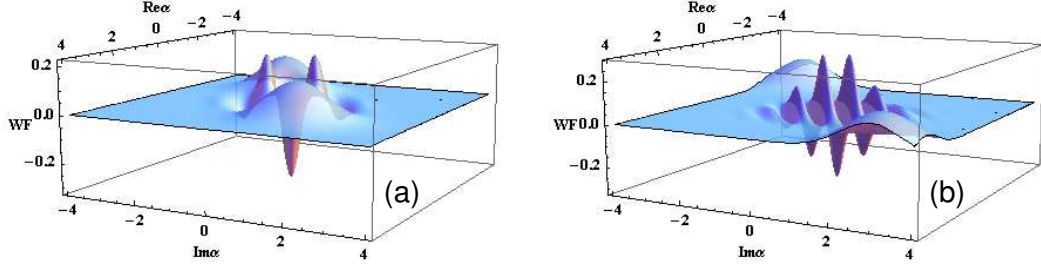


FIG. 7: Wigner function distributions of MCSO-OSCS with $m = 2, \varphi = 0$ (a) $\alpha_0 = 1 + i, \theta = \frac{\pi}{8}$; (b) $\alpha_0 = 2(1 + i), \theta = \frac{\pi}{3}$.

negative part of WF distribution for MCSO-OSCS, we shall consider the negative part volume of WF which may be written as

$$\delta = \frac{1}{2} \left[\int d^2\alpha |W(\alpha)| - 1 \right]. \quad (36)$$

By definition, the quantity δ is equal to zero for coherent and squeezed vacuum states, as their WFs are non-negative. Once knowing the Wigner function of a quantum state, we can obtain the negative part volume of WF through numerical integration.

In Fig. 8, we plot the negative part volume δ of WF for MCSO-OSCS as the function of θ . It is shown that the negative part volume δ generally increases as θ increases when $m \neq 0$. In addition, it is interesting to note that δ is sensitive to parameter m , and δ increases as m increases when parameter θ is bigger than a threshold (see Fig. 8(a)). In other words, the MCSO-OSCS may exhibit more nonclassicality by increasing the value of m . Meanwhile, δ increases as the value of α_0 increases when parameter θ is smaller than a threshold (see Fig. 8(b)).

VI. THE DECOHERENCE OF THE MCSO-OSCS IN A THERMAL ENVIRONMENT

When the MCSO-OSCS evolves in the thermal channel, the evolution of the density matrix in the Born-Markov approximation and the interaction picture can be described by the master equation [47]

$$\frac{d\rho}{dt} = \kappa(\bar{n} + 1) (2a\rho a^\dagger - a^\dagger a\rho - \rho a^\dagger a) + \kappa\bar{n} (2a^\dagger \rho a - aa^\dagger \rho - \rho aa^\dagger), \quad (37)$$

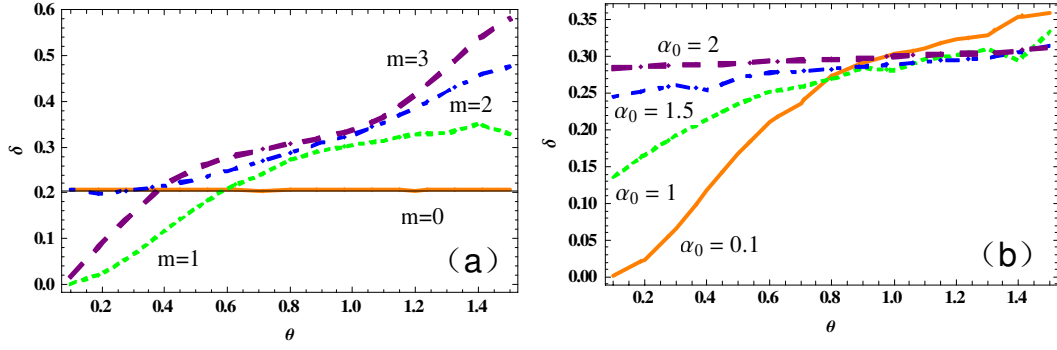


FIG. 8: The volume of the negative part of the WF for MCSO-OSCS as the function of θ (a) $\alpha_0 = 0.1, \varphi = 0$; (b) $m = 1, \varphi = 0$.

where κ represents the dissipative coefficient and \bar{n} ($\bar{n} = \frac{1}{e^{\hbar\omega/(k_B T)} - 1}$, T is temperature.) denotes the average thermal photon number of the environment [48]. Using the thermal entangled state representation [49], the time evolution of distribution functions in the dissipative channels are derived [50, 51]. The evolutions of the WF is governed by the following integration equation

$$W(\gamma, \gamma^*, t) = \frac{2}{(2\bar{n} + 1)\Gamma} \int \frac{d^2\alpha}{\pi} W(\alpha, \alpha^*, 0) \exp \left[-2 \frac{|\gamma - \alpha e^{-\kappa t}|^2}{(2\bar{n} + 1)\Gamma} \right], \quad (38)$$

where $\Gamma = 1 - e^{-2\kappa t}$ and $W(\alpha, \alpha^*, 0)$ is the WF of the initial state. Thus the WF at any time can be obtained by performing the integration when the initial WF is known.

Substituting Eq. (33) into Eq. (38), we have

$$W(\gamma, \gamma^*, t) = W_{\alpha_0}(\gamma, \gamma^*, t) + W_{-\alpha_0}(\gamma, \gamma^*, t) - (W'_{\alpha_0}(\gamma, \gamma^*, t) + c.c.), \quad (39)$$

where

$$W_{\alpha_0}(\gamma, \gamma^*, t) = \sum_{k=0}^m \sum_{l=0}^{m-k} M V U^l e^{-2V|\gamma - \alpha_0 e^{-\kappa t}|^2} |H_{m-k-l}(-C^* + R\alpha_0 U + R\gamma e^{-\kappa t} V)|^2, \quad (40)$$

$$\begin{aligned} W'_{\alpha_0}(\gamma, \gamma^*, t) = & \sum_{k=0}^m \sum_{l=0}^{m-k} M V U^l e^{(-2|\gamma|^2 V - 2|\alpha_0|^2 U + 2\gamma e^{-\kappa t} \alpha_0^* V - 2\gamma^* e^{-\kappa t} \alpha_0 V)} \\ & \times H_{m-k-l}(-B^* + R^* \alpha_0^* U + R^* \gamma^* e^{-\kappa t} V) H_{m-k-l}(B - R\alpha_0 U + R\gamma e^{-\kappa t} V), \end{aligned} \quad (41)$$

and

$$\begin{aligned} V &= \frac{1}{2\bar{n}\Gamma + 1}, U = 1 - e^{-2\kappa t} V, \\ M &= \frac{N_m^{-1} (-1)^k 2^{2l+k-m} (m!)^2 \sin^{k+l+m} \theta}{\pi k! l! ((m-k-l)!)^2 \cos^{k+l-m} \theta}. \end{aligned} \quad (42)$$

Further, when $t = 0, \Gamma = 0$, Eq.(39) just reduces to (33), as expected.

In order to see the decoherence of the MCSO-OSCS in the thermal environment, we plot the time evolution of WF $W(\gamma, \gamma^*, t)$ as a function of real and imaginary parts of γ for some different t values and for a given m value (say, $m = 1$) in Figs. 9. It is shown that as time proceeds the negative part of WF and multi-peaks vibration structure of the plot disappear gradually, and finally the plot evolves to a wave packet structure, the figure of a Gaussian distribution (see Fig. 9(d)), which means that the MCSO-OSCS has reduced to the thermal state. In Fig. 10, we plot the picture of $W(\gamma, \gamma^*, t)$ for some different \bar{n} values and for a given m value (say, $m = 1$) at the given time (say, $\kappa t = 0.05$). It is interesting to note that the negative part of WF decreases as the average photon number \bar{n} increases, i.e., the larger \bar{n} the more rapidly the nonclassicality is lost, which means that the higher the temperature of thermal field, the more rapidly the nonclassicality of the MCSO-OSCS is lost. This result is same as Ref. [52].

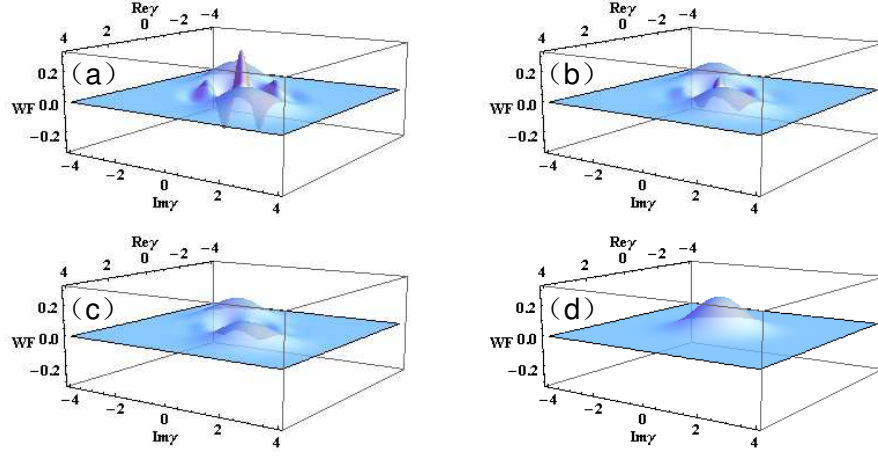


FIG. 9: The time evolution of Wigner function for MCSO-OSCS in the thermal environment with $\varphi = 0, \theta = \frac{\pi}{3}, \alpha_0 = 1 + i, m = 1, \bar{n} = 0.2$ (a) $\kappa t = 0.001$; (b) $\kappa t = 0.05$; (c) $\kappa t = 0.1$; (d) $\kappa t = 3$.

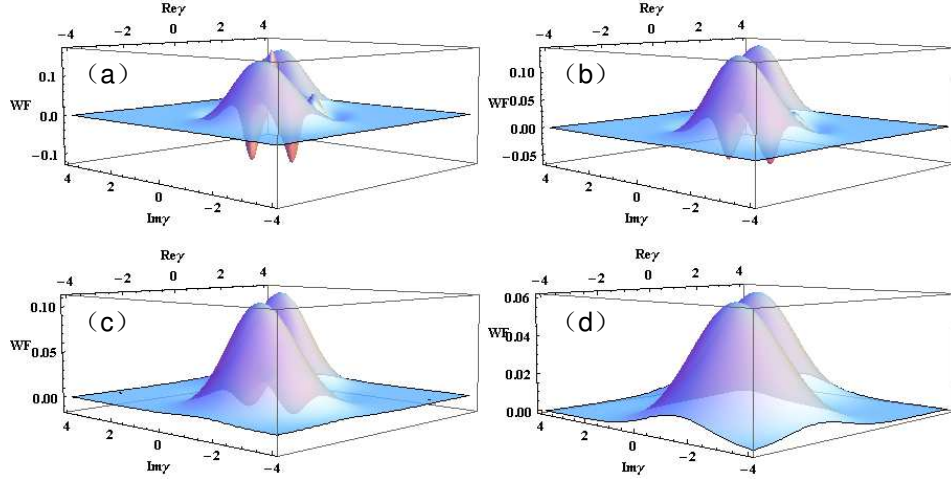


FIG. 10: Wigner function distributions of MCSO-OSCS in the thermal environment for $\varphi = 0, \theta = \frac{\pi}{3}, \alpha_0 = 1 + i, m = 1, \kappa t = 0.05$ with different parameter \bar{n} (a) $\bar{n} = 0$; (b) $\bar{n} = 0.5$; (c) $\bar{n} = 2$; (d) $\bar{n} = 8$.

VII. CONCLUSIONS

In summary, we investigate the nonclassicality of MCSO-OSCS which is obtained through m times coherent superposition operator $a \cos \theta + a^\dagger e^{i\varphi} \sin \theta$ operating on an odd-Schrödinger-cat state. For arbitrary m value, through IWOP technique we have obtained an analytical expression of the normalization constant, which turns out to be related with the Hermite polynomial. Then the fidelity between MCSO-OSCS and its original OSCS is discussed. By numerical plot, it is obvious to note that the fidelity is equal to 0 when m is odd and not equal to 0 when m is even. The nonclassical properties of the state, such as sub-Poissonian statistics, quadrature squeezing properties, and photocount distribution are also discussed in details. We find that MCSO-OSCS has more chance to exhibit sub-Poissonian statistics with bigger value of θ in the area of $\theta \in (0, \frac{\pi}{2})$. We also find that MCSO-OSCS can exhibit squeezing when the parameter m is odd and the angle θ is smaller, which indicates that the subtracting photon operation is benefit to squeezing for odd m . Furthermore, the nonclassicality of MCSO-OSCS is investigated in terms of WF and the negative part volume of WF after deriving the analytical expression of WF. It is shown that the WF of the MCSO-OSCS always has negative values which implies the highly nonclassical properties of quantum states. The negative part volume of WF increases as m increases when $m \neq 0$ and parameter θ is bigger than a threshold, and increases as the value of α_0 increases when parameter θ is smaller than a threshold. Especially, the negative part volume of WF increases with the increment of parameter θ except the case of $m = 0$.

We also investigate the decoherence of the MCSO-OSCS in terms of the fadeaway of the negativity of WF in a

thermal environment. It is shown that nonclassicality of the MCSO-OSCS decreases as time proceeds and the MCSO-OSCS reduces to the thermal state finally. It is also shown that nonclassicality is influenced by the temperature of environment, the higher the temperature is, the more rapidly the nonclassicality of the MCSO-OSCS is lost. We wish that our results will benefit for instructing experiments, for example, the new state would become a sufficient resource to generate a two-mode entanglement via a beam-splitter.

Acknowledgments

This project was supported by the National Natural Science Foundation of China (Nos.11264016, 11364022) and the Natural Science Foundation of Jiangxi Province of China (No.20142BAB202004) as well as the Research Foundation of the Education Department of Jiangxi Province of China (Nos.GJJ12171, GJJ12172).

-
- [1] Kim, M. S.: Recent developments in photon-level operations on travelling light fields. *J. Phys. B. -At. Mol. Opt. Phys.* **41**, 133001 (2008)
 - [2] Asboth, J. K., Calsamiglia, J., Ritsch, H.: Computable Measure of Nonclassicality for Light. *Phys. Rev. Lett.* **94**, 173602-1–173602-4 (2005)
 - [3] Kim, M. S., Park, E., Knight, P. L., Jeong, H.: Nonclassicality of a photon-subtracted Gaussian field. *Phys. Rev. A* **71**, 043805 (2005)
 - [4] Hu, L.-Y., Zhang, Z.-M.: Statistical properties of coherent photon-added two-mode squeezed vacuum and its inseparability. *J. Opt. Soc. Am. B*, **30**(3), 518-529 (2013)
 - [5] Guo, Q., Huang, L., Hu, L.-Y., Xu, X.-X., Zhang, H.-L.: Nonclassicality of Coherent Photon-Subtracted Two Single-Modes Squeezed Vacuum State. *Int. J. Theor. Phys.* **52**, 2886-2903 (2013)
 - [6] Parigi, V., Zavatta, A., Kim, M., Bellini, M.: Probing Quantum Commutation Rules by Addition and Subtraction of Single Photons to/from a Light Field. *Science* **317**, 1890 (2007)
 - [7] Boyd, R. W., Chan, K. W., O'Sullivan, M. N.: Quantum weirdness in the lab. *Science* **317**, 1874 (2007)
 - [8] Hu, L.-Y., Xu, X.-X., Wang, Z.-S., Xu, X.-F.: Photon-subtracted squeezed thermal state: Nonclassicality and decoherence. *Phys. Rev. A* **82**, 043842 (2010)
 - [9] Nha, H., Carmichael, H. J.: Proposed Test of Quantum Nonlocality for Continuous Variables. *Phys. Rev. Lett.* **93**, 020401 (2004)
 - [10] Takahashi, H., S. Neergaard-Nielsen, J., Takeuchi, M., Takeoka, M., Hayasaka, K., Furusawa, A., Sasaki, M.: Entanglement distillation from Gaussian input states. *Nature Photonics* **4**, 178 (2010).
 - [11] Agarwal, G. S., Tara, K.: Nonclassical properties of states generated by the excitations on a coherent state. *Phys. Rev. A* **43**, 492 (1991)
 - [12] Wenger, J., Tualle-Broui, R., Grangier, P.: Non-Gaussian Statistics from Individual Pulses of Squeezed Light. *Phys. Rev. Lett.* **92**, 153601 (2004)
 - [13] Zavatta, A., Viciani, S., Bellini, M.: Quantum-to-Classical Transition with Single-Photon-Added Coherent States of Light. *Science* **306**, 660 (2004)
 - [14] Lee, S.-Y., Nha, H.: Quantum state engineering by a coherent superposition of photon subtraction and addition. *Phys. Rev. A* **82**, 053812 (2010)
 - [15] Xu, X.-X., Yuan, H.-C., Hu, L.-Y., Fan, H.-Y.: Statistical properties of a generalized photon-modulated thermal state. *J. Phys. A: Math. Theor.* **44**, 445306 (2011)
 - [16] Yuan, H.-C., Xu, X.-X., Fan, H.-Y.: Generalized photon-added coherent state and its quantum statistical properties. *Chin. Phys. B* **19**, 104205 (2010)
 - [17] Dodonov, V. V., Malkon, I. A., Man'ko, V. I.: Even and odd coherent states and excitations of a singular oscillator. *Physica* **72**, 597 (1974)
 - [18] Wenger, J., Hafezi, M., Grosshans, F., Tualle-Broui, R., Grangier, P.: Maximal violation of Bell inequalities using continuous-variable measurements. *Phys. Rev. A* **67**, 012105 (2003)
 - [19] Jeong, H., Son, W., Kim, M. S., Ahn, D., Brukner, Č.: Quantum nonlocality test for continuous-variable states with dichotomic observables. *Phys. Rev. A* **67**, 012106 (2003)
 - [20] Ralph, T. C., Gilchrist, A., Milburn, G. J., Munro, W. J., Glancy, S.: Quantum computation with optical coherent states. *Phys. Rev. A* **68**, 042319 (2003)
 - [21] Jeong, H., Kim, M. S., Lee, J.: Quantum-information processing for a coherent superposition state via a mixed entangled coherent channel. *Phys. Rev. A* **64**, 052308 (2001)
 - [22] Munro, W. J., Nemoto, K., Milburn, G. J., Braunstein, S. L.: Weak-force detection with superposed coherent states. *Phys. Rev. A* **66**, 023819 (2002)
 - [23] Joo, J., Munro, W. J., Spiller, T. P.: Quantum Metrology with Entangled Coherent States. *Phys. Rev. Lett.* **107**, 083601 (2011).
 - [24] Ourjoumtsev, A., Jeong, H., Tualle-Broui, R., Grangier, Ph.: Generation of optical 'Schrödinger cats' from photon number states. *Nature (London)* **448**, 784 (2007).

- [25] Takahashi, H., Wakui, K., Suzuki, S., Takeoka, M., Hayasaka, K., Furusawa, A., Sasaki, M.: Generation of Large-Amplitude Coherent-State Superposition via Ancilla-Assisted Photon Subtraction. *Phys. Rev. Lett.* **101**, 233605 (2008).
- [26] Ourjoumtsev, A., Ferreyrol, F., Tualle-Brouiri, R., Grangier, Ph.: Preparation of non-local superpositions of quasi-classical light states. *Nat. Phys.* **5**, 189 (2009).
- [27] Gerrits, T., Glancy, S., Clement, T. S., Calkins, B., Lita, A. E., Miller, A. J., Migdall, A. L., Nam, S.W., Mirin, R. P., Knill, E.: Generation of optical coherent-state superpositions by number-resolved photon subtraction from the squeezed vacuum. *Phys. Rev. A* **82**, 031802 (2010).
- [28] Lee, C.-W., Lee, J., Nha, H., Jeong, H.: Generating a Schrödinger-cat-like state via a coherent superposition of photonic operations. *Phys. Rev. A* **85**, 063815 (2012)
- [29] Cai, Z.-B., Xu, B., Zhou, B., Wang, Z.-Y., Yang, Y.-F.: Nonclassical properties of states engineered via coherent operation of photon subtraction and addition on superpositions of coherent states. *Opt. Commun.* **311**, 229-233 (2013)
- [30] Rainville, E. D.: *Special Functions*. MacMillan, New York (1960)
- [31] Klauder, J. R., Skargerstam, B. S.: *Coherent States*. World Scientific, Singapore (1985)
- [32] Fan, H.-Y., Lu, H.-L., Fan, Y.: Newton–Leibniz integration for ket–bra operators in quantum mechanics and derivation of entangled state representations. *Ann. Phys.* **321**, 480 (2006)
- [33] Glauber, R. J.: The Quantum Theory of Optical Coherence. *Phys. Rev.* **130**, 2529 (1963)
- [34] Glauber, R. J.: Coherent and Incoherent States of the Radiation Field. *Phys. Rev.* **131**, 2766 (1963)
- [35] Lee, J., Kim, M. S., Jeong, H.: Transfer of nonclassical features in quantum teleportation via a mixed quantum channel. *Phys. Rev. A* **62**, 032305 (2000)
- [36] Chizhov, A. V., Knöll, L., Welsch, D.-G.: Continuous-variable quantum teleportation through lossy channels. *Phys. Rev. A* **65**, 022310 (2002)
- [37] Marek, P., Jeong, H., Kim, M. S.: Generating “squeezed” superpositions of coherent states using photon addition and subtraction. *Phys. Rev. A* **78**, 063811 (2008)
- [38] Agarwal, G. S., Tara, K.: Nonclassical character of states exhibiting no squeezing or sub-Poissonian statistics. *Phys. Rev. A* **46**, 485 (1992)
- [39] Hong, C. K., Mandel, L.: Generation of higher-order squeezing of quantum electromagnetic fields. *Phys. Rev. A* **32**, 974 (1985)
- [40] Lee, J., Kim, J., Nha, H.: Demonstrating higher-order nonclassical effects by photon-added classical states: realistic schemes. *J. Opt. Soc. Am. B, Opt. Phys.* **26**, 1363 (2009)
- [41] Orszag, M.: *Quantum Optics*. Springer, Berlin (2000)
- [42] Fan, H.-Y., Hu, L.-Y.: Two quantum-mechanical photocount formulas. *Opt. Lett.* **33**, 443 (2008)
- [43] Wigner, E. P.: On the quantum correction for thermodynamic equilibrium. *Phys. Rev.* **40**, 749-759 (1932)
- [44] Fan, H.-Y., Zaidi, H. R.: Application of IWOP technique to the generalized Weyl correspondence. *Phys. Lett. A* **124**, 303-307 (1987)
- [45] Schleich, W. P.: *Quantum Optics in Phase Space*. Wiley-VCH, Weinheim, (2001)
- [46] Bialynicki-Birula, I., Cirone, M. A., Dahl, J. P., Fedorov, M., Schleich, W. P.: In- and Outbound Spreading of a Free-Particle s-Wave. *Phys. Rev. Lett.* **89**, 0604041 (2002)
- [47] Jeong, H., Lee, J., Kim, M. S.: Dynamics of nonlocality for a two-mode squeezed state in a thermal environment. *Phys. Rev. A* **61**, 052101 (2000)
- [48] Hu, L.-Y., Xu, X.-X., Fan, H.-Y.: Statistical properties of photon-subtracted two-mode squeezed vacuum and its decoherence in thermal environment. *J. Opt. Soc. Am. B, Opt. Phys.* **27**, 286–299 (2010)
- [49] Fan, H.-Y., Hu, L.-Y.: *Entangled State Representation of Quantum Decoherence of the Open System*. Shanghai Jiaotong University Press, Shanghai (2010)
- [50] Hu, L.-Y., Chen, F., Wang, Z.-S., Fan, H.-Y.: Time evolution of distribution functions in dissipative environments. *Chin. Phys. B* **20**, 074204 (2011)
- [51] Hu, L.-Y., Wang, Q., Wang, Z.-S., Xu, X.-X.: Kraus Operator-Sum Representation and Time Evolution of Distribution Functions in Phase-Sensitive Reservoirs. *Int. J. Theor. Phys.* **51**, 331 (2012)
- [52] Huang, L., Guo, Q., Xu, X.-X., Yuan, W.: Nonclassicality and Decoherence of the Variable Arcsine State in a Thermal Environment. *Int. J. Theor. Phys.* **53**, 6 (2014)